IEEE Access
Multidisciplinary | Rapid Review | Open Access Journal

Received June 13, 2020, accepted June 18, 2020, date of publication June 24, 2020, date of current version August 4, 2020.

Digital Object Identifier 10.1109/ACCESS.2020.3004685

Optimal Selection of Rotor Bar Number in Multiphase Cage Induction Motors

GOJKO JOKSIMOVIĆ[1], (Senior Member, IEEE), MARIO MEZZAROBBA[2], ALBERTO TESSAROLO[2], (Senior Member, IEEE), AND EMIL LEVI[3], (Fellow, IEEE)

[1]Faculty of Electrical Engineering, University of Montenegro, 81000 Podgorica, Montenegro
[2]Engineering and Architecture Department, University of Trieste, 34127 Trieste, Italy
[3]Faculty of Engineering and Technology, Liverpool John Moores University, Liverpool L3 5UG, U.K.

Corresponding author: Gojko Joksimović (gojko.joksimovic@ucg.ac.me)

This work was supported in part by the Ministry of Science of Montenegro under Grant "Induction motor efficiency improvement through optimal electromagnetic design solutions - IMEI," and in part by the Faculty of Electrical Engineering, University of Montenegro.

ABSTRACT Rules for the selection of rotor bar numbers which minimize current and torque ripples are derived in this paper for a general symmetrical multiphase cage induction machine with prime phase number and integral slot winding. Analytically obtained expressions for optimal rotor bar number selection are validated by means of totally independent simulations, one based on a parameterized winding function (PWF) model of the induction machine and the other employing time-stepping finite-element analysis (TSFEA). As a case study, five-phase four-pole cage induction motors with forty stator slots and different number of rotor bars are comparatively analyzed. Results obtained from the PWF model are in excellent accordance with those independently obtained by TSFEA and both confirm the correctness of the proposed selection criteria. The practical motivation of the study is that an incorrect selection of rotor bar number can lead to parasitic torques of significant amplitude and, presently, there are no general rules available in the literature which may guide designers towards an optimal design choice for a general number of phases.

INDEX TERMS Induction machines, multiphase stator winding, parasitic torques, rotor slot harmonics, skewing, winding function model.

I. INTRODUCTION

Symmetrical induction machines with a number of phases greater than three are today commonly referred to as multiphase induction machines. Multiphase induction machines have various advantages over their conventional three-phase counterpart, such as lower space harmonic content, higher efficiency and torque density, better torque waveform, possibility to use time harmonics for output power production and multi-motor drive arrangements [1].

As exclusively inverter-fed machines, multiphase cage induction machines have been previously analyzed as parts of variable frequency drives [1], in conjunction with multiphase inverters and machine control strategies [2]–[5], parameter identification and estimation techniques [6]–[9], and modelling and operation under different fault conditions [10]–[12]. Very few papers, such as [13]–[16], have analyzed multiphase induction machines from the design standpoint, although design rules commonly adopted for three-phase machines cannot – in the majority of cases – be straightforwardly extended to the multiphase domain.

In [13] authors explore multiphase induction machines in order to determine the benefits that may be obtained from the motor point of view. They conclude that the main contribution of multiphase technology for increased efficiency results from a potential reduction in stator copper loss. Additionally, they recommend avoiding excitation harmonics of order $2mn \pm 1$, where m is the phase number and n is an integer, whenever possible, since these are the lowest order harmonics that produce torque ripple. In [14] the authors address the magnitude of rotor slot harmonics (RSHs) and highlight how they can be exploited in multiphase induction machines with sensorless control for speed estimation. This feature makes it desirable, for speed sensorless control purposes, to have large RSHs, although at the expense of increased Joule losses [14]. Different stator winding

The associate editor coordinating the review of this manuscript and approving it for publication was Pinjia Zhang.

This work is licensed under a Creative Commons Attribution 4.0 License. For more information, see https://creativecommons.org/licenses/by/4.0/

layouts are investigated and suggested in [15] and [16] for five- and nine-phase machines. Among other design aspects the authors highlight harmful influence of non-adequate number of rotor bars on parasitic torque components as well as on rotor slot harmonics in stator current spectrum.

The practical motivation of the present work arises from the observation that, as power electronics and control technologies advance, multiphase machines, although always inverter-fed, can be supplied by voltage sources which are closer and closer to the sinusoidal waveform, especially in the case of large medium-voltage motors fed from multilevel inverters. This makes the impact of supply source harmonics less and less harmful and, at the same time, gives more relevance to the need for improving motor performance with the same targets as in the grid-supplied, three-phase motors, [17]–[23].

In such a context, it can be of interest to design the multiphase machine so that parasitic phenomena which arise in the ideal case of a sinusoidal supply are minimized or, at least, reduced within acceptable limits. In particular, the presence of RSHs, although beneficial for the purpose of some sensorless control strategies, should be avoided or limited as a cause of significant deterioration of motor performance in terms of Joule losses, torque pulsations and electromagnetic noise.

In this regard, the paper will show that in a symmetrical multiphase cage induction motor, with a prime phase number and a generic number of poles and stator slots, RSH effects can be cancelled through a suitable selection of the rotor bar number, even without resorting to rotor bar skewing. A simple formula will be derived that provides the numbers of rotor bars that can be chosen to avoid space RSHs and thus minimize current and torque ripples.

The proposed criterion is first validated through a recently developed parameterized winding function (PWF) model, [24], which has been shown capable of reliably and quickly predicting the performance of multi-phase induction motors with both straight and skewed rotor bars. As a further independent validation, time-stepping finite-element analysis (TSFEA) will be also used as a cross-check to confirm the results obtained from the PWF model.

To illustrate the practical application of the work, a four-pole five-phase cage induction motor with forty stator slots will be considered as a case study. Its performance will be investigated at steady state when different numbers of rotor bars are chosen, in case of both straight and skewed bar design [25]. This will serve the purpose of proving the effectiveness of the developed optimal design rule.

The paper is organized as follows. In Section II, the generation and properties of stator and rotor magnetic fields in a symmetrical multiphase induction motor will be reviewed. In Section III and IV, the impact of space RSHs on current and torque pulsations are, respectively, investigated in relation to the number of rotor bars. In Section V the rule is given for the optimal choice of the number of rotor bars leading to zero RSH-related torque and current pulsations. Finally, in Section VI the results of a case study based on a five-phase four-pole induction motor will be reported for different choices of rotor bar numbers, confirming the results of the introduced design rules through the use of the PWF model, which is further suitably validated against TSFEA simulations.

II. AIR-GAP FLUX SPACE HARMONICS

The stator current and torque ripples in multiphase machine under the assumption of sinusoidal supply have the origin in the harmonic content of the air-gap field produced by both stator and rotor currents.

The simplifying assumptions made in the study consist of considering a uniform air-gap and negligible magnetic saturation.

A. STATOR AIR-GAP FLUX SPACE HARMONICS

Let us consider a generic symmetrical multiphase cage induction motor with m phases (displaced by $2\pi/m$ radians apart), p pole pairs and

$$S = 2mpq \tag{1}$$

stator slots, where q is an integer representing the number of slots per pole per phase. In symmetrical steady-state conditions at $\omega = 2\pi f$ stator angular frequency, the stator phase current fundamentals are:

$$\begin{aligned} i_1^{(s)}(t) &= I\cos(\omega t), \quad i_2^{(s)}(t) = I\cos\left(\omega t - \tfrac{2\pi}{m}\right), \\ i_3^{(s)}(t) &= I\cos\left(\omega t - 2\tfrac{2\pi}{m}\right)\ldots i_m^{(s)}(t) \\ &= I\cos\left(\omega t - (m-1)\,\tfrac{2\pi}{m}\right) \end{aligned} \tag{2}$$

and the ν^{th} order flux-density harmonic they produce is [26]:

$$B_\nu^{(s)}(t,\theta) = B_{\max\,\nu}^{(s)} \sum_{k=0}^{m-1} \cos\left(\omega t - \nu p\theta + k\,(\nu-1)\,\tfrac{2\pi}{m}\right). \tag{3}$$

From (3) it can be noticed that the ν^{th} harmonic exists only on condition that

$$\nu \in \mathcal{U} = \{2mz + 1 : \ z \in \mathbb{Z}\}, \tag{4}$$

because, for any other value of ν, the sum in (3) is zero.

It is well known [27] that stator flux-density harmonics tend to decrease as the harmonic order $|\nu|$ grows and that the so-called stator slot harmonics can have significant amplitudes. Their harmonic order is $|\nu| = S/p \pm 1 = 2mq \pm 1$ and is obtained for $z = \pm q$ in (4). In general, harmonic orders corresponding to $-q \le z \le q$ in (4) are the most prominent, with the maximum being obviously associated with the fundamental ($z = 0$).

B. ROTOR AIR-GAP FLUX SPACE HARMONICS

The way how a rotor cage, equipped with R rotor bars and revolving with a slip s with respect to the fundamental of the air-gap field, reacts to each flux-density harmonic produced by the stator is the same as for three-phase machines and

has been already investigated in the literature [28]. It has been demonstrated that the stator μ^{th} flux-density harmonic induces rotor currents which, in turn, generate a rotating flux-density wave given by,

$$\begin{aligned} &B_{\mu}^{(r)}(t,\theta_r) \\ &= \sum_{r=0}^{R-1} \sum_{\eta=1,2,3,\ldots} B_{\max\mu,\eta}^{(r)} \left[\cos\left(s_\mu \omega t + \eta\theta_r - r(\eta+\mu p)\frac{2\pi}{R}\right)\right. \\ &\left. + \cos\left(s_\mu \omega t - \eta\theta_r + r(\eta-\mu p)\frac{2\pi}{R}\right)\right], \end{aligned} \tag{5}$$

where $\mu \in \mathcal{U}$, $B_{\max\mu,\eta}^{(r)}$ are Fourier coefficients which can be computed as per [28], s_μ is

$$s_\mu = 1 - \mu(1-s) \tag{6}$$

and θ_r is the angular coordinate in a rotor-attached reference frame such that

$$\theta - \theta_r = \tfrac{1-s}{p}\omega t. \tag{7}$$

Current ripples arise in stator currents due to some rotor harmonics (5) being linked by stator phases and inducing electromotive forces in them [28]. Pulsating torques arise from any possible interaction between the sets of harmonics (3) and (5).

The most significant harmonics in the rotor field are those corresponding to the fundamental of the stator field ($\mu = 1$). Furthermore, it is known that remarkable disturbances in both currents and torques can result from the space RSHs, which are obtained from (5) when

$$\eta = \lambda R \pm \mu p, \tag{8}$$

with λ being a positive integer, i.e. [28]:

$$B_L^{RSH}(t,\theta_r) = B_{\max,L}^{RSH}\cos\left(s_\mu\omega t + (\lambda R - \mu p)\theta_r\right), \tag{9}$$
$$B_U^{RSH}(t,\theta_r) = B_{\max,U}^{RSH}\cos\left(s_\mu\omega t - (\lambda R + \mu p)\theta_r\right). \tag{10}$$

Using (6) and (7) in (9)-(10) we obtain:

$$\begin{aligned} B_L^{RSH}(t,\theta) = B_{\max,L}^{RSH}\cos\left(\left(1-\lambda\tfrac{R}{p}(1-s)\right)\omega t\right. \\ \left. + \left(\tfrac{\lambda R}{p} - \mu\right)p\theta\right), \end{aligned} \tag{11}$$

$$\begin{aligned} B_U^{RSH}(t,\theta) = B_{\max,U}^{RSH}\cos\left(\left(1+\lambda\tfrac{R}{p}(1-s)\right)\omega t\right. \\ \left. - \left(\tfrac{\lambda R}{p} + \mu\right)p\theta\right). \end{aligned} \tag{12}$$

The amplitude of rotor slot harmonics can be usually significant for low values of λ and μ and, in particular, for $\mu = 1$ and $1 \le \lambda \le 4$.

Since (11)-(12) depend on the number of rotor bars R, it is intuitive that an appropriate selection of R can help reduce the effects of (11)-(12) on stator currents and air-gap torque, as investigated in the next Section.

III. ROTOR SLOT HARMONICS IN PHASE CURRENTS

As a general rule, an air-gap flux density space harmonic having a generic number of pole pairs n can produce electromotive forces and induce currents in the stator winding only if the stator winding itself can produce an air-gap flux density harmonic like (3) having the same number of pole pairs [29].

For instance, (11) produces stator current pulsations, having frequency

$$f_L^{RSH} = \left|1 - \lambda\tfrac{R}{p}(1-s)\right| f, \tag{13}$$

if there exists a stator harmonic of order $\nu_L \in \mathcal{U}$ having the same number of pole pairs as (11), which happens if

$$\pm\left(\tfrac{\lambda R}{p} - \mu_L\right) = \nu_L \in \mathcal{U} \tag{14}$$

for a given $\lambda \in \mathbb{Z}^+$ and a given $\mu_L \in \mathcal{U}$. Similarly, (12) produces stator current pulsations, having frequency

$$f_U^{RSH} = \left|1 + \lambda\tfrac{R}{p}(1-s)\right| f, \tag{15}$$

if there exists a stator harmonic of order $\nu_U \in \mathcal{U}$ having the same number of pole pairs as (12), which happens if

$$\pm\left(\tfrac{\lambda R}{p} + \mu_U\right) = \nu_U \in \mathcal{U}. \tag{16}$$

for a given $\lambda \in \mathbb{Z}^+$ and a given $\mu_U \in \mathcal{U}$.

Therefore, lower RSH currents will appear if there exist two integers z_{L1} and z_{L2} such that

$$\pm\left[\tfrac{\lambda R}{p} - (2z_{L1}m + 1)\right] = (2z_{L2}m + 1), \tag{17}$$

while upper RSH currents will appear if there exist two integers z_{U1} and z_{U2} such that:

$$\pm\left[\tfrac{\lambda R}{p} + (2z_{U1}m + 1)\right] = (2z_{U2}m + 1). \tag{18}$$

From (17) we have that the rotor bar numbers R leading to lower RSH currents are such that,

$$\lambda R \in \mathcal{R}_L^+ \cup \mathcal{R}_L^-, \tag{19}$$

where

$$\begin{aligned} \mathcal{R}_L^+ &= \left\{2p\left(m\, z_L^+ + 1\right),\ \ z_L^+ \in \mathbb{Z}^+\right\}, \\ \mathcal{R}_L^- &= \left\{2p\, m\, z_L^-,\ \ z_L^- \in \mathbb{Z}^+\right\}, \end{aligned} \tag{20}$$

with the substitution $z_L^+ = |z_{L2} + z_{L1}|$ and $z_L^- = |z_{L2} - z_{L1}|$ without any loss of generality.

The two sets $\mathcal{R}_L^+$ and $\mathcal{R}_L^-$ are respectively obtained choosing the sign "+" and the sign "−" in (14) and (17).

Similarly, the rotor bar numbers R leading to upper RSH currents are such that,

$$\lambda R \in \mathcal{R}_U^+ \cup \mathcal{R}_U^-, \tag{21}$$

where

$$\begin{aligned} \mathcal{R}_U^+ &= \left\{2pmz_U^+,\ \ z_U^+ \in \mathbb{Z}^+\right\}, \\ \mathcal{R}_U^- &= \left\{2p\left(mz_U^- - 1\right),\ \ z_U^- \in \mathbb{Z}^+\right\}, \end{aligned} \tag{22}$$

with the substitution $z_U^+ = |z_{U2} - z_{U1}|$ and $z_U^- = |z_{U2} + z_{U1}|$ with no loss of generality.

The two sets $\mathcal{R}_U^+$ and $\mathcal{R}_U^-$ are respectively obtained choosing the sign "+" and the sign "−" in (16) and (18).

Finally, the rotor bar numbers R leading to both lower and upper RSH currents are such that

$$\lambda R \in \mathcal{R}_{LU} = \left(\mathcal{R}_L^+ \cup \mathcal{R}_L^-\right) \cap \left(\mathcal{R}_U^+ \cup \mathcal{R}_U^-\right), \tag{23}$$

where it can be easily seen that

$$\mathcal{R}_{LU} = \mathcal{R}_L^- = \mathcal{R}_U^+ \tag{24}$$

because $\mathcal{R}_L^+ \cap \mathcal{R}_L^- = \emptyset$.

To summarize, we can say that the space RSHs (11)-(12) for a given $\lambda \in \mathbb{Z}^+$ cause current pulsations if λR falls in one of the three sets $\mathcal{R}_L^+$, $\mathcal{R}_U^-$ and $\mathcal{R}_{LU}$: depending on whether λR belongs to $\mathcal{R}_L^+$, $\mathcal{R}_U^-$ or $\mathcal{R}_{LU}$, current pulsations will arise having frequency, respectively, $\left|1 - \lambda\frac{R}{p}(1-s)\right| f$, $\left|1 + \lambda\frac{R}{p}(1-s)\right| f$ or both.

In practical cases, the most prominent pulsations obviously arise from the flux density harmonics which are usually obtained for $1 < \lambda < 4$ and for z_{L1}, z_{L2}, z_{U1} and z_{U2} in (17)-(18) between -q and q, leading to z_L^+, z_L^-, z_U^+, z_U^- values in (20) and (22) between 1 and 2q (it can be easily seen that zero for these variables does not lead to feasible numbers of rotor bars).

IV. ROTOR SLOT HARMONICS IN TORQUE

As a general rule, two generic air-gap flux density space harmonics

$$B_s(t,\theta) = B_{s,\max}\cos\left(2\pi f_s t - n_s\theta_r\right), \tag{25}$$
$$B_r(t,\theta) = B_{r,\max}\cos\left(2\pi f_r t - n_r\theta_r\right), \tag{26}$$

(with $f_s > 0$ and $f_r > 0$), respectively, produced by the stator and rotor currents, can interact producing electromagnetic torque on condition that they have the same number of poles, i.e. $n_s = \pm n_r$ and, in this case, the resulting torque will have a pulsation given by $|f_s \mp f_r|$ [30].

In particular, (11) for a given λ will interact with the stator space harmonic of order $\nu_L \in \mathcal{U}$ and produce torque if (14) holds for some value of $\mu_L \in \mathcal{U}$. It is worth noticing that the sign "+" in (14) applies when the two interacting harmonics revolve in the opposite direction, as it can be seen comparing (11) and (5), while the sign "−" applies when the two harmonics revolve in the same direction. Following the same reasoning as in the previous Section, we can observe that (11) produces torque pulsation for numbers of rotor bars R satisfying (17) and the torque pulsation will have frequency

$$f_0^{torque} = \left|1 - \left(1 - \lambda\frac{R}{p}(1-s)\right)\right| f = \lambda\frac{R}{p}(1-s)f \tag{27}$$

when

$$\lambda R \in \mathcal{R}_L^- = \mathcal{R}_{LU} \tag{28}$$

(harmonic fields rotating in the same direction), while the torque pulsation will have frequency

$$f_L^{torque} = \left|1 + \left(1 - \lambda\frac{R}{p}(1-s)\right)\right| f = \left|2 - \lambda\frac{R}{p}(1-s)\right| f \tag{29}$$

when

$$\lambda R \in \mathcal{R}_L^+ \tag{30}$$

(harmonic fields rotating in the opposite direction).

Similarly, (12) for a given λ will interact with the stator space harmonic of order $\nu_U \in \mathcal{U}$ and produce torque if (16) holds for some value of $\mu_U \in \mathcal{U}$. It is worth noticing that the sign "+" in (16) applies when the two interacting harmonics revolve in the same direction, as it can be seen comparing (12) and (5), while the sign "−" applies if the two harmonics revolve in the opposite direction. Following again the same reasoning as in the previous Section, we can observe that (12) produces torque pulsation for numbers of rotor bars R satisfying (21) and the torque pulsation will have frequency

$$f_0^{torque} = \left|1 - \left(1 + \lambda\frac{R}{p}(1-s)\right)\right| f = \lambda\frac{R}{p}(1-s)f \tag{31}$$

when

$$\lambda R \in \mathcal{R}_U^+ \tag{32}$$

(harmonic fields rotating in the same direction), while the torque pulsation will have frequency

$$f_U^{torque} = \left|1 + \left(1 + \lambda\frac{R}{p}(1-s)\right)\right| f = \left|2 + \lambda\frac{R}{p}(1-s)\right| f \tag{33}$$

when

$$\lambda R \in \mathcal{R}_U^- \tag{34}$$

(harmonic fields rotating in the opposite direction).

To summarize, we can say that the space RSHs (11)-(12) for a given $\lambda \in \mathbb{Z}^+$ cause torque pulsations if λR falls in one of the three sets $\mathcal{R}_L^+$, $\mathcal{R}_U^-$ and $\mathcal{R}_{LU}$: depending on whether λR belongs to $\mathcal{R}_L^+$, $\mathcal{R}_U^-$ or $\mathcal{R}_{LU}$, the torque pulsation will, respectively, have frequency $\left|2 - \lambda\frac{R}{p}(1-s)\right| f$, $\left|2 + \lambda\frac{R}{p}(1-s)\right| f$ or $\lambda\frac{R}{p}(1-s)f$. It is noted that in the latter case ($\lambda R \in \mathcal{R}_{LU}$), a torque pulsation is produced at a frequency equal to the average of current RSH frequencies $\left|1 - \lambda\frac{R}{p}(1-s)\right| f$ and $\left|1 + \lambda\frac{R}{p}(1-s)\right| f$.

V. RULE FOR OPTIMAL ROTOR BAR SELECTION

The results obtained in the two previous Sections lead to the conclusion that the absence of current and torque pulsations due to RSHs in a multiphase cage induction motor with m phases can be guaranteed by choosing the number of rotor bars R so that

$$\lambda R \notin \mathcal{R}_L^+ \cup \mathcal{R}_U^- \cup \mathcal{R}_{LU} \quad \forall\lambda \in \mathbb{Z}^+. \tag{35}$$

Using (20), (22) and (24), the condition above can be more explicitly formulated as follows:

$$\lambda R \notin 2p\,(mz + c) \quad \forall\lambda,\ z \in \mathbb{Z}^+,\ c = \{-1,\ 0,\ 1\}. \tag{36}$$

This can be equivalently stated saying that, to guarantee the absence of the RSH-related current and torque pulsations,

the number of rotor bars R must not be either a divisor of $2pmz$ or a divisor of $2p(mz \pm 1)$ for any positive integer z.

As previously noted, in practical applications only pulsations resulting from significant harmonics need to be taken into account, which makes it reasonable to limit the investigation to such typical ranges as $1 \leq \lambda \leq 4$ and $1 \leq z \leq 2q$ ($z = 0$ leads to unfeasible number of rotor bars). Since $1 \leq z \leq 2q$ and considering (1), one can notice that the number $2p\,(mz + c)$ in (36) varies between $2p(m-1)$ and $2p\,[m\,(2q)+1] = 2\,(S+p)$; then the restriction given by (36) for the choice of R make sense only if,

$$2p\,(m-1) < \lambda R < 2(S+p) \tag{37}$$

that is

$$2p\,(m-1)/\lambda < R < 2\,(S+p)/\lambda. \tag{38}$$

If we now consider that $1 \leq \lambda \leq 4$, we have

$$1/4 \leq 1/\lambda \leq 1 \tag{39}$$

and combining (38) and (39):

$$p\,(m-1)/2 < R < 2\,(S+p)\,. \tag{40}$$

In other words, it can be said that, in order to avoid potentially harmful current and torque pulsation, the number of rotor bars R should be chosen that is a not a divisor of either $2p(mz \pm 1)$ or $2pmz$ for any positive integer z between 1 and $2q$. Mathematically, R should then satisfy the following,

$$R \nmid 2p\,(mz + c) \quad \forall z,\ c \in \mathbb{Z},\quad 1 \leq z \leq 2q,\quad -1 \leq c \leq 1. \tag{41}$$

where mathematical symbol means $\nmid$ "does not divide".

VI. APPLICATION EXAMPLE AND CASE STUDY

As a case study to illustrate the application of the novel design rule, a five-phase ($m = 5$) four-pole ($p = 2$) cage induction motor with $S = 40$ ($q = 2$) stator slots will be taken as an example. To guarantee the absence of RSH-related current and torque pulsations, the number of rotor bars R needs to be chosen so that it is not a divisor of either $2pmz$ or $2p(mz \pm 1)$ for all z between 1 and $2q = 4$. The significant range for the selection of R is between $p(m-1)/2 = 4$ and $2(S+p) = 84$. Values of R included in such a range and satisfying the condition (41) are such that

$$R \in \mathcal{R}_{even} \cup \mathcal{R}_{odd}, \tag{42}$$

where

$$\mathcal{R}_{even} = \left\{ \begin{matrix} 26, 34, 46, 48, 50, 52, 54, 58, \\ 62, 66, 68, 70, 72, 74, 78, 82 \end{matrix} \right\}, \tag{43}$$

$$\mathcal{R}_{odd} = \left\{ \begin{matrix} 17, 23, 25, 27, 29, 31, 33, 35, 37, 39, 41, \\ 43, 45, 47, 49, 51, 53, 55, 57, 59, 61, 63, 65, \\ 67, 69, 71, 73, 75, 77, 79, 81, 83 \end{matrix} \right\}. \tag{44}$$

In the usual design of induction motors, an even number of rotor bars is generally preferred to minimize unbalanced magnetic forces in the radial direction [31], [32]. Therefore, only the rotor bar numbers belonging to the set $\mathcal{R}_{even}$ will be considered.

In order to validate the theory and design criteria discussed in the previous Section, the performance of the five-phase four-pole induction motor with forty stator slots, i.e. $S = 40$, is simulated for different possible choices of R. More detailed data for the simulated machine are provided in Table 1. Operation with rated load is considered at all times.

TABLE 1. Characteristic data of the example induction motor.

Rated power	7.5 kW
Rated voltage	400 V
Rated frequency	50 Hz
Rated speed	1458 rpm
Phase connection	star
Rated power factor	0.85
Rated efficiency	0.9
Coil to pole pitch ratio	9/10
Number of coils per phase	8
Number of turns per coil	24
Rotor inertia	0.025 kg m^2
Stator phase resistance	1.821 Ω
Stator phase leakage inductance	12.78 mH
Rotor bar resistance at 80°C	63.58 μΩ
Rotor end-ring segment resistance at 80°C	1.48 μΩ
Rotor bar leakage inductance	401.39 nH
Rotor end-ring segment leakage inductance	4.56 nH

The data reported in Table 1 refer to the particular case where the machine rotor is equipped with $R = 30$ rotor bars. When changing the number of bars in PWF model, the design is left unchanged except for adjusting the bar dimensions according to the criteria which are reported in [24] and summarized in the Appendix.

For the purpose of motor simulation, the PWF induction machine model described in [24] is used because it is numerically efficient and it also offers the possibility of comparatively exploring a wide variety of design variants (with both skewed and unskewed rotor bars) with reasonable computational effort. The reliability of the model for the analysis of induction machines in transient and steady-state conditions has already been confirmed by comparison against commercially available FEM software, [33], [34]. Also, in preparing this work, the authors have made extensive comparisons between motor performance predicted through the PWF model and from TSFEA finding a very good matching in all cases (an example of such comparisons will be provided in the following).

Fig. 1 shows the stator winding MMFs at an instant of time, assuming unit value of phase currents, as well as its harmonic spectral content. Harmonic orders correspond to those predicted according to (4): 1st, 9th, 11th are the 2nd, 18th and 22nd in Fig. 1. The most prominent space harmonics are the first order stator slot harmonics, whose orders are $(S/p \pm 1)$ the 19th and 21st (the 38th and 42nd in Fig. 1), as observed in Section II.A.

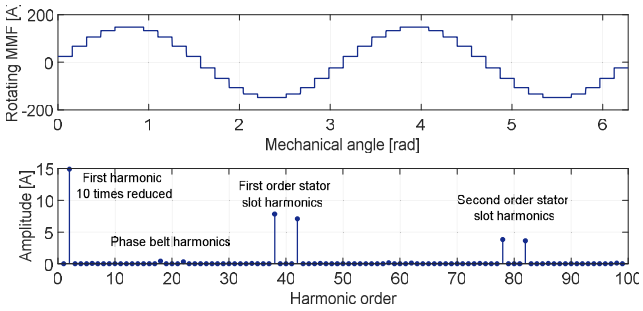

FIGURE 1. Rotating MMF wave of a symmetrical five-phase four-pole stator winding placed into $S = 40$ stator slots and its spectral content for the example machine assumed as a case study.

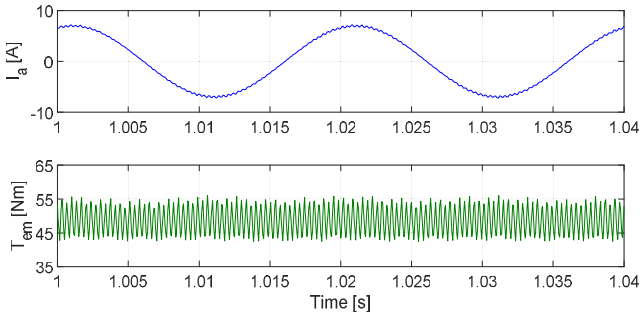

FIGURE 2. Stator phase current (top) and developed electromagnetic torque (bottom) in steady-state conditions for a machine with $R = 30$ unskewed rotor bars (results from the PWF model): $s = 0.027$.

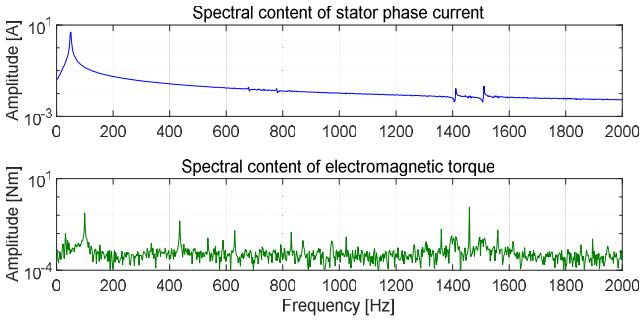

FIGURE 3. Spectral content of the stator phase current (top) and developed electromagnetic torque (bottom) in steady-state conditions for a machine with $R = 30$ unskewed rotor bars (results from the PWF model): $s = 0.027$.

As a first example, the behavior of the machine with a number of rotor bars $R = 30$ is considered. Fig. 2 shows the stator phase current and electromagnetic torque in full-load steady-state conditions for the machine with $R = 30$ unskewed rotor bars, while Fig. 3 shows the relevant spectral contents (the DC torque component, equal to the rated torque, 48.72 Nm, is removed).

Since $R = 30$ does not belong to the set of optimal rotor bar numbers (43), pulsations are expected both in stator currents and in the torque. Indeed, both RSHs at $f_L^{RSH} = 1410$ Hz and $f_U^{RSH} = 1510$ Hz, corresponding to (13) and (15) for $\lambda = 2$, are clearly visible in the current spectrum. This is fully consistent with the theory given in Section III because $\lambda R = 60$ belongs to the set (23) i.e. set (41) for $z = 3$ and $c = 0$. A pulsating torque at the frequency $f_0^{torque} = 1460$ Hz, given by (27) and (31) for $\lambda = 2$, is also clearly visible in the torque spectrum at the mean frequency of the RSH currents for the same λ, as predicted in Section III.

As a second example, the behaviour of the motor is investigated for a number of rotor bars $R = 54$, which belongs to the set of preferred numbers of rotor bars according to (43). It will be shown later that this number of rotor bars is not only preferred but even optimal as it produces minimal value of the electromagnetic torque ripple in the analysed range $20 < R < 60$. Rotor speed and developed electromagnetic torque during a full-load start-up transient of the motor fed with constant rated voltage are shown in Fig 4. The current and torque waveforms with relevant spectra are shown in Fig. 5 and Fig. 6. In accordance with the analytically derived predictions, significant RSHs do not appear in either the stator current or in the torque.

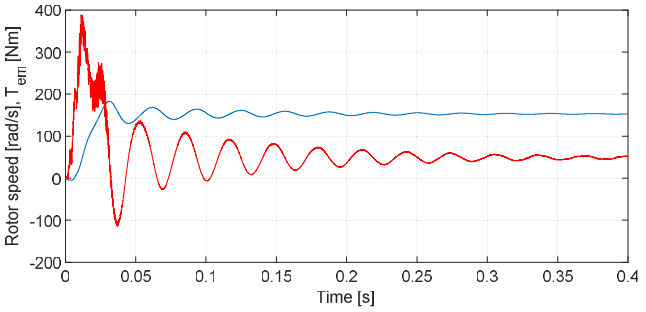

FIGURE 4. Rotor speed and developed electromagnetic torque during start-up of the fully loaded motor for a machine with $R = 54$ unskewed rotor bars (results from the PWF model).

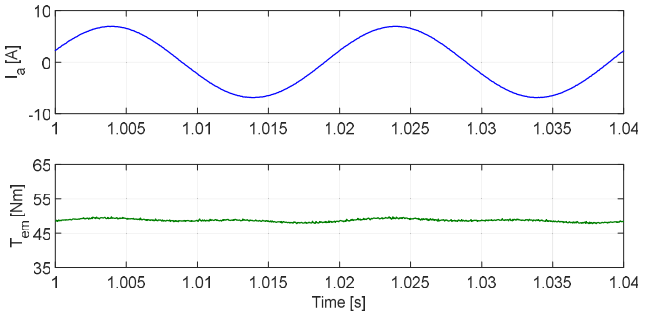

FIGURE 5. Stator phase current (top) and developed electromagnetic torque (bottom) in steady-state conditions for machine with $R = 54$ unskewed rotor bars – results from the PWF model.

In order to demonstrate the reliability of the PWF model, a comparison is shown next between the results obtained from the PWF model and those resulting from the TSFEA simulation of the same machine. Both simulations are run for the case of $R = 28$ rotor bars, which is not among the optimal values as per (43). Fig. 7 and Fig. 8 show the comparison between the transient currents and speed of the motor from the two simulation approaches during an electromechanical transient. The transient is the acceleration with rated load

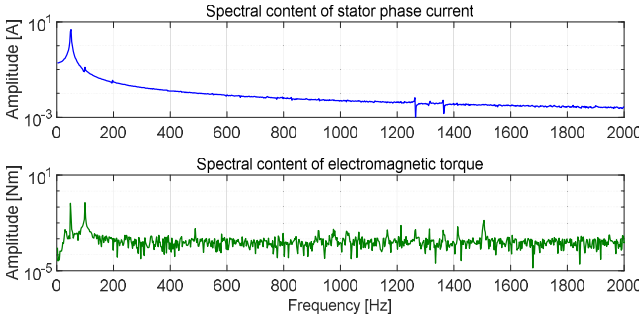

FIGURE 6. Spectral content of stator phase current (top) and developed electromagnetic torque (bottom) in steady-state conditions for machine with $R = 54$ unskewed rotor bars – results from PWF model.

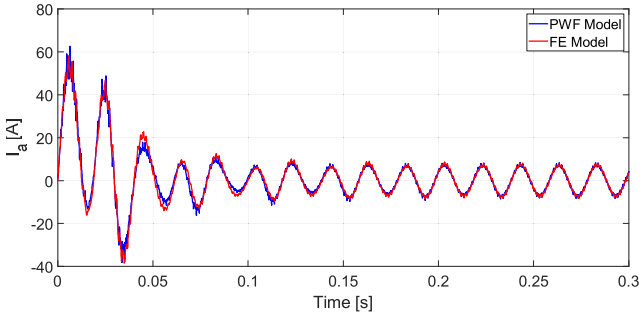

FIGURE 7. Stator phase current during transient obtained using PWF and TSFEA simulations with $R = 28$ unskewed rotor bars.

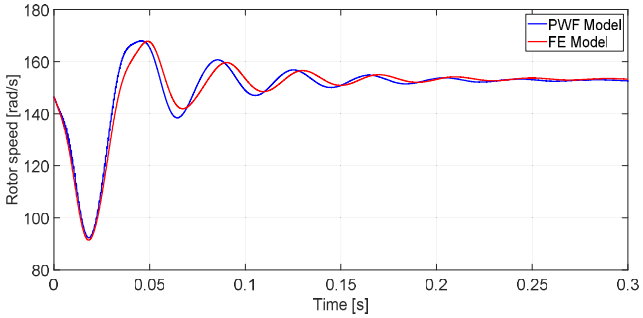

FIGURE 8. Rotor speed during transient obtained using PWF and TSFEA simulations with $R = 28$ unskewed rotor bars.

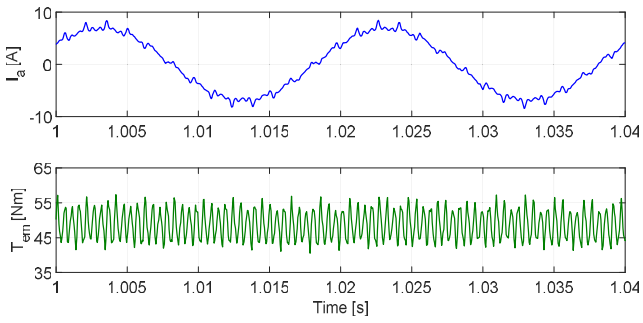

FIGURE 9. Stator phase current (top) and developed electromagnetic torque (bottom) in steady-state conditions for the machine with $R = 28$ unskewed rotor bars: results from the PWF model.

torque and the rotor position and rotor speed (1400 rpm) at $t = 0$ are set the same in both PWF and TSFEA models. Fig. 9 and Fig. 10 show phase current and torque waveforms at steady state from the two simulations.

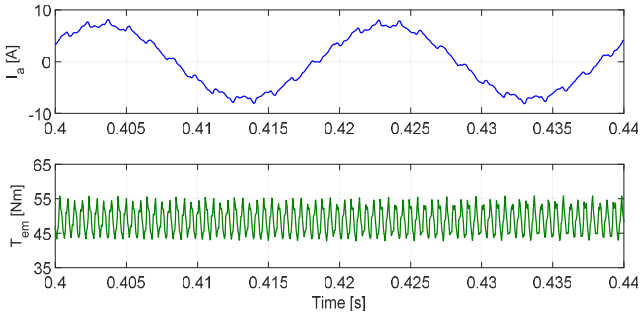

FIGURE 10. Stator phase current (top) and developed electromagnetic torque (bottom) in steady-state conditions for the machine with $R = 28$ unskewed rotor bars: results from the TSFEA model.

A very satisfactory matching can be observed in the results from the two completely independent and structurally different models. However, the TSFEA requires several hours or days for a single simulation to complete, while the same result can be obtained with the PWF model almost instantaneously. Furthermore, the PWF makes it possible to simulate the motor behaviour in the presence of rotor bar skewing [25], [35], which would require a 3D approach, or several 2D simulations with suitable subsequent post-processing, if TSFEA were used.

The flexibility and computational efficiency of the PWF model also make it a very effective tool to rapidly collect and compare performance results relating to a wide variety of designs. For instance, what is presented next is an overview of the example motor performance in terms of torque pulsations when the number of rotor bars R varies between 20 and 60. In order to have a relatively easy comparison, a torque ripple factor is defined as [33],

$$r\,(\%) = \frac{T_{em,AC,RMS}}{T_{em,DC}} \cdot 100 \tag{45}$$

where $T_{em,DC}$ is the average (useful) torque computed by integration over a period T,

$$T_{em,DC} = \frac{1}{T} \int_{t_0}^{t_0+T} T_{em}\,(t)\,dt \tag{46}$$

and $T_{em,AC,RMS}$ is the RMS value of the torque:

$$T_{em,AC,RMS} = \sqrt{\frac{1}{T} \int_{t_0}^{t_0+T} \left(T_{em}\,(t) - T_{em,DC}\right)^2 dt} \tag{47}$$

Results are given in Table 2 and represented graphically in Fig. 11, where, for each number of rotor bars, the design with unskewed bars and the design with bars skewed by one stator slot pitch are taken into account.

First of all, it can be seen how bar skewing leads to a drastic reduction in torque pulsations. However, in some cases (especially for large medium voltage machines) bar skewing can introduce manufacturing complications as well as a production cost increase. Furthermore, it is known how

TABLE 2. Torque ripple factor for different numbers of skewed and unskewed rotor bars in the analysed five-phase four-pole induction motor: $m = 5$, $p = 2$, $S = 40$, $20 \leq R \leq 60$.

	R=20	R=22	R=24	R=26	R=28	R=30	R=32
r (%), *skewed*	1.495	0.918	0.694	0.575	0.613	0.653	0.579
r (%), unskewed	43.121	17.272	10.127	2.428	8.192	7.618	6.057
	R=34	**R=36**	**R=38**	**R=40**	**R=42**	**R=44**	**R=46**
r (%), *skewed*	0.443	1.231	0.769	0.728	0.881	1.169	0.702
r (%), unskewed	0.940	21.531	7.558	57.522	6.524	23.162	1.314
	R=48	**R=50**	**R=52**	**R=54**	**R=56**	**R=58**	**R=60**
r (%), *skewed*	0.576	0.587	0.856	0.603	0.864	0.822	0.941
r (%), unskewed	1.684	1.963	3.116	0.897	1.921	6.507	10.261

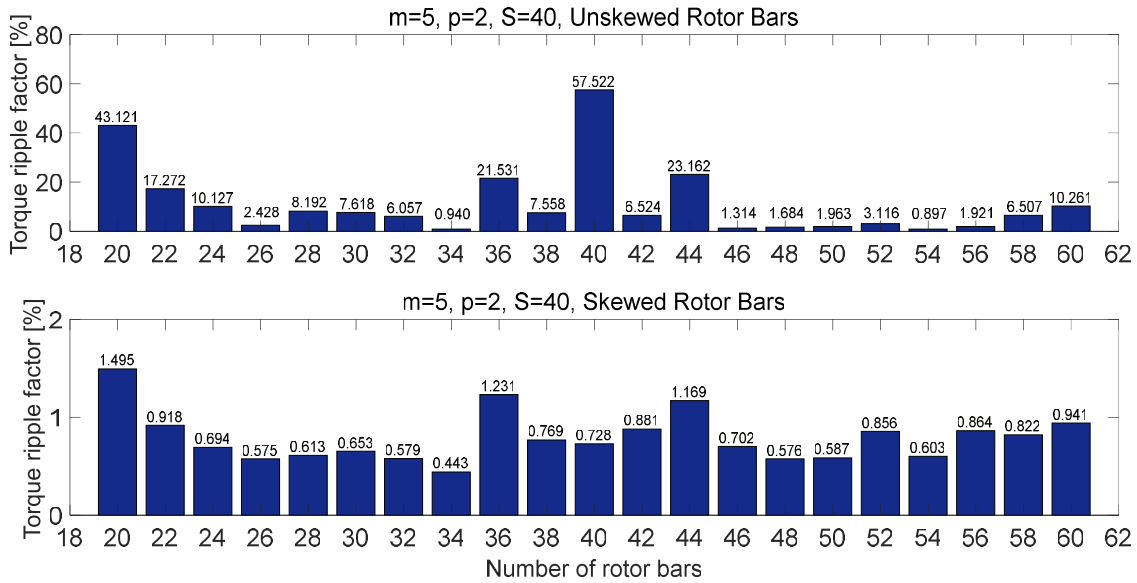

FIGURE 11. Torque ripple factor for unskewed (top) and skewed (bottom) rotor bars in five-phase four-pole cage rotor induction motor: $m = 5$, $p = 2$, $S = 40$, $20 \leq R \leq 60$.

rotor bar skewing, in addition to benefits, gives also rise to possible problems, such as inter-bar currents and occurrence of undesired axial field components, resulting in both core and Joule additional losses [36]. Therefore, the possibility to obtain very small torque pulsations without skewing, i.e. through a proper selection of the number of rotor bars, can represent a significant advantage.

In this sense, Fig. 11 for the unskewed bar design shows that there are rotor bar numbers for which an extremely small torque pulsation is achieved. If we compare the numerical results summarized in Fig. 11 with the optimal bar numbers (43) resulting from the proposed design criterion, we can observe that the minimum torque ripple factor is obtained only for the number of rotor bars theoretically identified as optimal.

As an additional criterion of goodness of rotor bar selection, total harmonic distortion (THD) of stator phase current was calculated, according to the THD definition

$$THD\,(\%) = \frac{\sqrt{I_{s2}^2 + I_{s3}^2 + I_{s4}^2 + \dots}}{I_{s1}} \cdot 100 \qquad (48)$$

where I_{sn} is the RMS value of n^{th} harmonic of stator phase current and $n = 1$ is the fundamental harmonic. This has been done only for the case of unskewed rotor bars because, when the rotor bars are skewed, the THD is smaller than 2% for any number of rotor bars. Results are given in Table 3 and represented graphically in Fig. 12. In almost all cases, the number of rotor bars that yields the smallest torque ripple also leads to small values of THD. One exception is the case with $R = 48$ rotor bars, where a rather high value of the THD is obtained. The reason for this high value is currently unclear and will be a subject of further investigations.

TABLE 3. Total harmonic distortion (THD) of stator phase current for different numbers of unskewed rotor bars in the analysed five-phase four-pole induction motor: $m = 5$, $p = 2$, $S = 40$, $20 \leq R \leq 60$.

	R=20	R=22	R=24	R=26	R=28	R=30	R=32
THD (%), unskewed	13.318	13.834	12.368	2.132	8.675	1.886	21.586
	R=34	**R=36**	**R=38**	**R=40**	**R=42**	**R=44**	**R=46**
THD (%), unskewed	1.334	32.878	6.225	32.106	6.288	33.889	1.023
	R=48	**R=50**	**R=52**	**R=54**	**R=56**	**R=58**	**R=60**
THD (%), unskewed	18.466	1.925	5.089	0.764	5.451	5.357	4.071

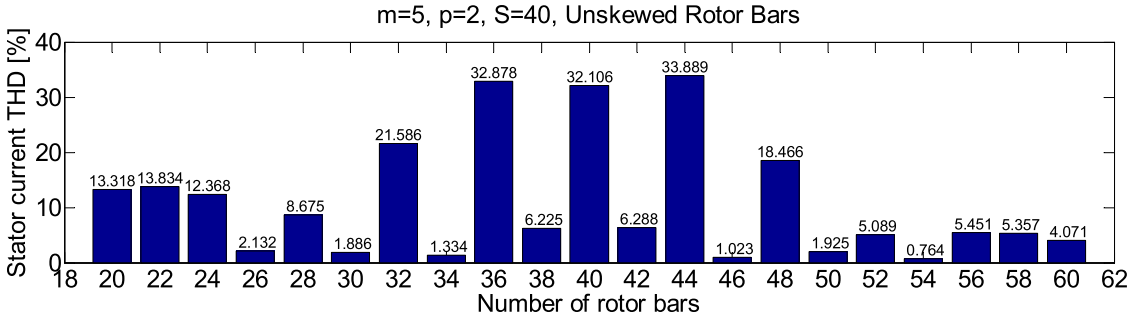

FIGURE 12. Total harmonic distortion of stator phase current for unskewed rotor bars in five-phase four-pole cage rotor induction motor: $m = 5$, $p = 2$, $S = 40$, $20 \leq R \leq 60$.

VII. DISCUSSION

One important remark is that the developed design rule, if particularized to three-phase cage induction motors ($m = 3$), leads to the same results already discussed in [33], as one can easily check numerically. This further corroborates the generality of the presented methodology.

A further point which may be worth discussing is that the selection of rotor bar number R is addressed in this paper considering electromagnetic torque ripple minimization as the only criterion. However, from a practical point of view it is clear that what the method yields is not a single value of R but a set of preferred values. It will be then up to the designer to identify the most suitable number R, among the preferred ones, considering also other criteria. For example, design configurations with many thin rotor bars may be advantageous from a thermal point of view thanks to the larger surface available for heat transfer by conduction between the cage and the surrounding laminations. Conversely, configurations with relatively few rotor bars may be preferred because they lead to a slightly lower Carter's coefficient [37] and, consequently, to a slightly improved power factor.

Last but not least, the rotor bar number selection criteria, derived in the paper, are valid if and only if the stator winding is with an integral slot winding. Hence fractional slot windings, which are anyway relatively seldom used in induction machines, are not encompassed by the analysis.

VIII. CONCLUSION

Multiphase cage induction motors are of increasing importance for the benefits they can bring in several respects, such as increased fault tolerance, efficiency, torque density and innovative control and drive arrangement solutions. With the advances of both power electronics and PWM inverter control technology, it is often possible to supply multiphase induction motors with a high-quality supply voltage, especially if multilevel inverter configurations are used. This tends to reduce PWM-related parasitic effects and give more importance to the performance issues which can result from possibly inappropriate choices made in the induction motor electromagnetic design. In this scenario, the paper has investigated the potentially harmful effects which can arise in a cage induction motor with an arbitrary number of symmetrically-distributed prime number of phases from the interaction of stator and rotor revolving fields, with special attention to the so-called rotor slot harmonics (RSHs).

It has been shown how RSH-related pulsations arise, in general, in both stator phase currents and air-gap torque at well-defined frequencies and with amplitudes that strongly depend on the number of rotor bars. A simple algebraic criterion has been derived and formulated to identify those (optimal) numbers of rotor bars which lead to zero RSH-related pulsations. The proposed design rule has been validated in the example case of a four-pole five-phase forty stator slot cage induction motor by studying its steady-state performance for different numbers of rotor bars. It has been shown how, even in the absence of bar skewing, current and torque pulsations can be practically eliminated if the number of rotor bars is chosen according to the introduced rule. It is believed that the findings of the paper will be of practical interest for multiphase machine designers.

APPENDIX

A brief summary of the recently derived parameterized winding function (PWF) model, [24], is given here, explaining how the motor cross section model is adapted in the PWF model to consider different numbers of rotor bars. An initial rotor design, such as that illustrated in Table 1, is first defined through the output-coefficient sizing approach [37] and assuming an arbitrary number R of rotor bars; R can be then changed so that the bar cross section A_{bar} and end-ring cross sections A_{ring} are proportional to $1/R$:

$$A_{bar} \propto \frac{1}{R}, \quad A_{ring} \propto \frac{1}{R \sin(p\pi/R)}. \tag{49}$$

In this way, the losses in the bars and end rings, the flux density in rotor teeth and the overall machine performance due to the fundamental of the air-gap field and useful torque production do not change.

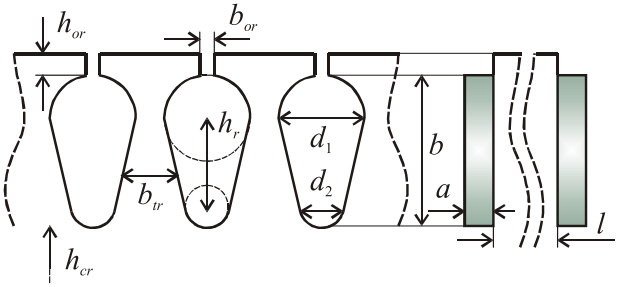

FIGURE 13. Rotor slot and cage details. In particular, *a* and *b* represent the end-ring cross section dimensions.

To have (49) satisfied, the dimensions shown in Fig. 13 are adjusted as follows,

$$b_{tr} = \frac{B_g \pi D_r}{k_{Fe} B_{tr} R} \tag{50}$$

$$d_1 = \frac{\pi (D_r - 2h_{or}) - R b_{tr}}{R + \pi} \tag{51}$$

$$d_2 = \sqrt{\frac{8CA_{bar} - (C\pi + 8) d_1^2}{C\pi - 8}} \tag{52}$$

$$h_r = 2(d_1 - d_2)/C \tag{53}$$

$$b = 1.1 (h_{or} + h_r + 0.5 (d_1 + d_2)) \tag{54}$$

$$a = A_{ring}/b \tag{55}$$

where

$$C = 4 \tan(\pi/R) \tag{56}$$

and D_r is rotor outer diameter, k_{Fe} is the stacking factor, and B_g and B_{tr} are the flux densities in the air gap and rotor teeth, respectively.

For any choice of R, the leakage inductances associated with a single bar and an end-ring segment connected to it are, respectively, computed as (l_{bar} is the bar length):

$$L_{bar} = \mu_0 l_{bar} \left(0.66 + \frac{2h_r}{3(d_1 + d_2)} + \frac{h_{or}}{b_{or}}\right) \tag{57}$$

$$L_{ring} = 0.46 \mu_0 \pi \frac{D_r - b}{R} \log\left(\frac{2.35 \cdot (D_r - b)}{2a + b}\right) \tag{58}$$

REFERENCES

[1] E. Levi, R. Bojoi, F. Profumo, H. A. Toliyat, and S. Williamson, "Multiphase induction motor drives—A technology status review," *IET Elect. Power Appl.*, vol. 1, no. 4, pp. 489–516, 2007.

[2] M. Jones, S. N. Vukosavic, D. Dujic, and E. Levi, "A synchronous current control scheme for multiphase induction motor drives," *IEEE Trans. Energy Convers.*, vol. 24, no. 4, pp. 860–868, Dec. 2009.

[3] M. Morawiec, P. Strankowski, A. Lewicki, J. Guzinski, and F. Wilczynski, "Feedback control of multiphase induction machines with backstepping technique," *IEEE Trans. Ind. Electron.*, vol. 67, no. 6, pp. 4305–4314, Jun. 2020.

[4] Z. Liu, Z. Zheng, Q. Wang, and Y. Li, "Enhanced rotor field-oriented control of multiphase induction machines based on symmetrical components theory," *IET Power Electron.*, vol. 12, no. 4, pp. 656–666, Apr. 2019.

[5] A. S. Abdel-Khalik, M. I. Masoud, and B. W. Williams, "Improved flux pattern with third harmonic injection for multiphase induction machines," *IEEE Trans. Power Electron.*, vol. 27, no. 3, pp. 1563–1578, Mar. 2012.

[6] A. G. Yepes, J. A. Riveros, J. Doval-Gandoy, F. Barrero, Ó. Lopez, B. Bogado, M. Jones, and E. Levi, "Parameter identification of multiphase induction machines with distributed windings—Part 1: Sinusoidal excitation methods," *IEEE Trans. Energy Convers.*, vol. 27, no. 4, pp. 1056–1066, Dec. 2012.

[7] J. A. Riveros, A. G. Yepes, F. Barrero, J. Doval-Gandoy, B. Bogado, O. Lopez, M. Jones, and E. Levi, "Parameter identification of multiphase induction machines with distributed windings—Part 2: Time-domain techniques," *IEEE Trans. Energy Convers.*, vol. 27, no. 4, pp. 1067–1077, Dec. 2012.

[8] J. Rodas, F. Barrero, M. R. Arahal, C. Martin, and R. Gregor, "Online estimation of rotor variables in predictive current controllers: A case study using five-phase induction machines," *IEEE Trans. Ind. Electron.*, vol. 63, no. 9, pp. 5348–5356, Sep. 2016.

[9] H. S. Che, A. S. Abdel-Khalik, O. Dordevic, and E. Levi, "Parameter estimation of asymmetrical six-phase induction machines using modified standard tests," *IEEE Trans. Ind. Electron.*, vol. 64, no. 8, pp. 6075–6085, Aug. 2017.

[10] A. G. Yepes, J. Doval-Gandoy, F. Baneira, and H. A. Toliyat, "Speed estimation based on rotor slot harmonics in multiphase induction machines under open-phase fault," *IEEE Trans. Power Electron.*, vol. 33, no. 9, pp. 7980–7993, Sep. 2018.

[11] H. Liu, D. Wang, and X. Yi, "Modeling and analytical calculation of a multiphase induction motor in the phase loss asymmetrical transient process," *J. Electr. Eng. Technol.*, vol. 14, no. 3, pp. 1269–1279, May 2019.

[12] J. Apsley and S. Williamson, "Analysis of multiphase induction machines with winding faults," *IEEE Trans. Ind. Appl.*, vol. 42, no. 2, pp. 465–472, Mar./Apr. 2006.

[13] S. Williamson and S. Smith, "Pulsating torque and losses in multiphase induction machines," *IEEE Trans. Ind. Appl.*, vol. 39, no. 4, pp. 986–993, Jul./Aug. 2003.

[14] A. G. Yepes, F. Baneira, J. Malvar, A. Vidal, D. Perez-Estevez, O. Lopez, and J. Doval-Gandoy, "Selection criteria of multiphase induction machines for speed-sensorless drives based on rotor slot harmonics," *IEEE Trans. Ind. Electron.*, vol. 63, no. 8, pp. 4663–4673, Aug. 2016.

[15] A. S. Abdel-Khalik, S. Ahmed, and A. M. Massoud, "Steady-state mathematical modeling of a five-phase induction machine with a combined star/pentagon stator winding connection," *IEEE Trans. Ind. Electron.*, vol. 63, no. 3, pp. 1331–1343, Mar. 2016.

[16] A. S. Abdel-Khalik, S. Ahmed, and A. M. Massoud, "A nine-phase six-terminal concentrated single-layer winding layout for high-power medium-voltage induction machines," *IEEE Trans. Ind. Electron.*, vol. 64, no. 3, pp. 1796–1806, Mar. 2017.

[17] G. Kron, "Induction motor slot combinations rules to predetermine crawling, vibration, noise and hooks in the speed-torque curve," *Trans. Amer. Inst. Electr. Eng.*, vol. 50, no. 2, pp. 757–767, Jun. 1931.

[18] T. Kobayashi, F. Tajima, M. Ito, and S. Shibukawa, "Effects of slot combination on acoustic noise from induction motors," *IEEE Trans. Magn.*, vol. 33, no. 2, pp. 2101–2104, Mar. 1997.

[19] B.-T. Kim, B.-I. Kwon, and S.-C. Park, "Reduction of electromagnetic force harmonics in asynchronous traction motor by adapting the rotor slot number," *IEEE Trans. Magn.*, vol. 35, no. 5, pp. 3742–3744, Sep. 1999.

[20] J. Le Besnerais, V. Lanfranchi, M. Hecquet, and P. Brochet, "Optimal slot numbers for magnetic noise reduction in variable-speed induction motors," *IEEE Trans. Magn.*, vol. 45, no. 8, pp. 3131–3136, Aug. 2009.

[21] K. N. Gyftakis and J. Kappatou, "The impact of the rotor slot number on the behaviour of the induction motor," *Adv. Power Electron.*, vol. 2013, Feb. 2013, Art. no. 837010.
[22] T. Gundogdu, Z. Q. Zhu, and J. C. Mipo, "Influence of rotor slot number on rotor bar current waveform and performance in induction machines," in *Proc. 20th Int. Conf. Electr. Mach. Syst. (ICEMS)*, Sydney, NSW, Australia, Aug. 2017, pp. 1–6, doi: 10.1109/ICEMS.2017.8055936.
[23] T. Gundogdu, Z. Q. Zhu, J. C. Mipo, and S. Personnaz, "Influence of rotor skew on rotor bar current waveform and performance in induction machines," in *Proc. 21st Int. Conf. Electr. Mach. Syst. (ICEMS)*, Jeju, South Korea, Oct. 2018, pp. 525–530.
[24] G. Joksimović, "Dynamic model of cage induction motor with number of rotor bars as parameter," *J. Eng.*, vol. 2017, no. 6, pp. 205–211, Jun. 2017.
[25] G. Joksimović, A. Kajević, S. Mujović, T. Dlabač, V. Ambrožič, and A. Tessarolo, "Rotor bar skewing impact on electromagnetic pulsations in cage induction motors," in *Proc. IcETRAN*, Srebrno Jezero, Serbia, 2019, pp. 292–296.
[26] J. Faiz, V. Ghorbanian, and G. Joksimović, *Fault Diagnosis of Induction Motors*. Edison, NJ, USA: IET, 2017.
[27] J. Pyrhonen, T. Jokinen, and V. Hrabovcova, *Design of Rotating Electrical Machines*. Hoboken, NJ, USA: Wiley, 2014.
[28] G. Joksimovic, M. Kjurovic, and J. Penman, "Cage rotor MMF: Winding function approach," *IEEE Power Eng. Rev.*, vol. 21, no. 4, pp. 64–66, Apr. 2001.
[29] G. M. Joksimovic, J. Riger, T. M. Wolbank, N. Peric, and M. Vasak, "Stator-current spectrum signature of healthy cage rotor induction machines," *IEEE Trans. Ind. Electron.*, vol. 60, no. 9, pp. 4025–4033, Sep. 2013.
[30] S. N. Vukosavić, *Electrical Machines*. New York, NY, USA: Springer-Verlag, 2012.
[31] A. Arkkio, "Unbalanced magnetic pull in cage induction motors with asymmetry in rotor structures," in *Proc. 8th Int. Conf. Electr. Mach. Drives (EMD)*, Cambridge, U.K., 1997, pp. 36–40.
[32] T. Aho, J. Nerg, and J. Pyrhonen, "The effect of the number of rotor slits on the performance characteristics of medium-speed solid rotor induction motor," in *Proc. 3rd IET Int. Conf. Power Electron., Mach. Drives (PEMD)*, 2006, pp. 515–519.
[33] G. Joksimović, J. I. Melecio, P. M. Tuohy, and S. Djurović, "Towards the optimal 'slot combination' for steady-state torque ripple minimization: An eight-pole cage rotor induction motor case study," *Electr. Eng.*, vol. 102, no. 1, pp. 293–308, Mar. 2020.
[34] G. Joksimović, A. Kajevic, M. Mezzarobba, and A. Tessarolo, "Optimal rotor bars number in four pole cage induction motor with 36 stator slots—Part I: Numerical modeling," in *Proc. Int. Conf. Elect. Mach. (ICEM)*, Gothenburg, Sweden, May 2020.
[35] J. M. Gojko, D. D. Momir, and O. B. Aleksandar, "Skew and linear rise of MMF across slot modelling-winding function approach," *IEEE Trans. Energy Convers.*, vol. 14, no. 3, pp. 315–320, Sep. 1999.
[36] C. I. McClay, "The influence of rotor skew on cage motor losses," in *Proc. 8th Int. Conf. Electr. Mach. Drives (EMD)*, Cambridge, U.K., 1997, pp. 263–267.
[37] I. Boldea and S. A. Nasar, *Induction Machines Design Handbook*. Boca Raton, FL, USA: CRC Press, 2002.

GOJKO JOKSIMOVIĆ (Senior Member, IEEE) received the M.Sc. and Ph.D. degrees in electrical power engineering from the University of Montenegro, Podgorica, Montenegro, in 1995 and 2000, respectively. Since May 2011, he has been a Professor at the University of Montenegro. He has authored some books, one international scientific monograph, and a number of articles published in leading international scientific journals. His main research interest includes mathematical modeling and analysis of electrical machines from condition monitoring and design optimization points of view. He was a recipient of the Alexander von Humboldt Research Fellowship.

MARIO MEZZAROBBA received the Laurea degree in electrical engineering from the University of Trieste, Trieste, Italy, in 2009, and the Ph.D. degree in electrical engineering from the University of Padova, Padua, Italy, in 2014. Since 2014, he has been a Research Fellow at the University of Trieste and has actively taken part in several research projects for the dimensioning, design, prototyping, and testing of electromechanical actuators, components, and systems. His main research interests include induction motors, permanent-magnet machines, and electromagnetic stirring analysis, design, and optimization.

ALBERTO TESSAROLO (Senior Member, IEEE) received the Laurea degree in electrical engineering from the University of Padova, in 2000, and the Ph.D. degree in electrical engineering from the University of Trieste, Italy, in 2011. Before joining the university, he was involved in the design and development of large innovative motors, generators, and drives. Since 2006, he has been with the Engineering and Architecture Department, University of Trieste, where he teaches the courses in electric machine fundamentals and electric machine design. He leads several funded research projects in cooperation with industrial companies for the study and development of innovative electric motors, generators, and drives. He has authored over 150 international articles in the areas of electrical machines and drives. He is a member of the Rotating Machinery Technical Committee TC2 (rotating electric machinery) of the International Electrotechnical Commission (IEC). He has been an Associate Editor of the IEEE TRANSACTIONS ON ENERGY CONVERSION, the IEEE TRANSACTIONS ON INDUSTRY APPLICATIONS, and *IET Electric Power Applications*. He is currently the Editor-in-Chief of the IEEE TRANSACTIONS ON ENERGY CONVERSION.

EMIL LEVI (Fellow, IEEE) received the M.Sc. and Ph.D. degrees in electrical engineering from the University of Belgrade, Yugoslavia, in 1986 and 1990, respectively. He joined Liverpool John Moores University, U.K., in May 1992, where he has been a Professor of electric machines and drives, since September 2000. He was a recipient of the Cyril Veinott Award of the IEEE Power and Energy Society, in 2009, and the Best Paper Award of the IEEE TRANSACTIONS ON INDUSTRIAL ELECTRONICS, in 2008. In 2014, he received the Outstanding Achievement Award from the European Power Electronics (EPE) Association, and in 2018, the Professor Istvan Nagy Award from the Power Electronics and Motion Control (PEMC) Council. He served as a Co-Editor-in-Chief of the IEEE TRANSACTIONS ON INDUSTRIAL ELECTRONICS, from 2009 to 2013. He is currently the Editor-in-Chief of the IEEE TRANSACTIONS ON INDUSTRIAL ELECTRONICS and the *IET Electric Power Applications* and an Editor of the IEEE TRANSACTIONS ON ENERGY CONVERSION.